Robotica (2013) volume 31, pp. 203–216. © Cambridge University Press 2012
doi:10.1017/S0263574712000185

A redundant dynamic model of parallel robots for model-based control

Asier Zubizarreta† Itziar Cabanes*,†, Marga Marcos† and Charles Pinto‡

†*Department of Automatic Control and System Engineering, University of the Basque Country, Spain*
‡*Department of Mechanical Engineering, University of the Basque Country, Spain*

(Accepted April 13, 2012. First published online: May 22, 2012)

SUMMARY
The use of extra sensors in parallel robots can provide an increase in control performance, making it possible to fully exploit the potential of these mechanisms. In this paper, a comprehensive redundant dynamic modelling procedure for the six-degree-of-freedom Gough platform is presented. The proposed methodology makes it possible to define the model in terms of all sensorized joint variables in order to implement redundant information-based control, and an example, the Extended Computed Torque Control (Extended CTC) approach, is developed. This, applied to parallel robots, ensures better dynamic performance than the traditional CTC approach. In order to validate dynamic modelling, a two-step procedure is used in this paper. First, the redundant dynamic model is validated by comparing its dynamic performance with the previous research in the field. Second, an exhaustive study is carried out that demonstrates the advantages of the redundant dynamic model when used in the Extended CTC approach.

KEYWORDS: Robot dynamics; Control of robotic systems; Mechatronic systems; Parallel manipulators; Sensor networks.

1. Introduction

Current industrial processes demand more accuracy, speed, and robustness in order to be competitive and increase product quality while reducing cycle time. Because of their flexibility and wide operational workspace, serial robots, based on arm-like mechanisms, have been used widely in industry. However, as their open-chain structure provides low stiffness, the bodies of these robots usually need to be bulky and heavy, significantly reducing both their ability to move at high speeds and their load/weight ratio. In turn, this strongly limits their use in tasks that require high-speed, precision, or heavy load handling.

In this context, where there is a need to design tools for executing specific tasks, industry has tended to focus on the recently rediscovered parallel robots.[32] In these mechanisms, a mobile platform with attached end-effector is, in turn, connected to a fixed platform by a set of serial kinematic chains or limbs. This structure provides high stiffness and a high load/weight ratio. In addition, in some parallel structures the actuators can be fixed to the base, reducing the moving mass of the mechanism and allowing higher operational speeds. Thus, these robots have been proposed as the best option when high-speed, precision, or heavy load handling are required.

One of the most popular parallel robots is the Gough platform (Fig. 1), a fully parallel, six-degree-of-freedom (6-DOF) robot created in 1947 by Dunlop Rubber Co.'s engineer Eric Gough.[18] The generalized mechanical structure is composed of a mobile platform joined with six $U\underline{P}S$ kinematic chains to a base platform. This robot is also known in related papers as the *Stewart platform*, *Stewart–Gough platform*, or *Gough–Stewart platform*, considering it a generalization of the 6-DOF flight simulator designed by Stewart.[38]

The Gough platform has all the characteristic strengths of parallel mechanisms, making it suitable for tasks that require heavy load handling[39] or high accuracy.[12,33] Because of the popularity of this robot, some unconventional applications can also be found in the literature, such as in inspection of tubular structures[3] and underwater observation tasks.[45]

The complex structure of the Gough platform does, however, present some challenges, and these have restricted its use in industrial applications. First, its closed-chain structure limits the workspace, making it smaller than the one offered by 6-DOF serial robots. Second, depending on the geometry and dimensions of the robot, the workspace may contain singularities, meaning that there are regions where the robot becomes uncontrollable. Finally, the kinematics and dynamics of the Gough platform are highly coupled and their solution requires numerical methods due to the presence of non-actuated joints. In order to solve these issues and fully exploit the capabilities of the Gough platform, extensive research has been conducted in recent years. Nevertheless, although important advances have been made in the areas of kinematics, synthesis, and workspace analysis, other areas, such as control and dynamics, have been less well studied due to the complexity of the formulation.[10]

Regarding the formulation of the dynamics of the Gough platform, the main proposals in this area can be grouped into three approaches. The first group is based on the classical Newton–Euler formulation in which all the forces applied

* Corresponding author. E-mail: asier.zubizarreta@ehu.es

https://doi.org/10.1017/S0263574712000185 Published online by Cambridge University Press

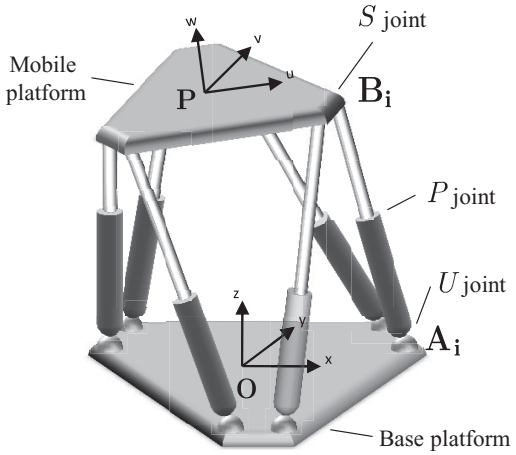


Fig. 1. Schematic of the Gough platform.

to all components of the mechanism have to be considered, leading to a high dimension problem.[9,11,24,28,37] The second group applies the Lagrangian formulation, an energetic approach that avoids the calculation of internal forces of the mechanism.[1,6,7,19,27] The third group uses the Principle of Virtual Work, which is also an energetic approach[14,15] and provides the most efficient unstructured dynamic model from the point of view of computation time.[41,42] From analysis of related research in the field of dynamics, three main conclusions could be drawn. First, the compact dynamic model of the Gough platform can be calculated using any of these three approaches. Second, the dynamics of the Gough platform are naturally calculated as the contribution of dynamics of two subsystems: the mobile platform and the serial chains. Finally, the dynamic model of the serial chains can be easily parallelized in multiprocessor computers, as all limbs are structurally identical.

While there are some publications detailing the dynamics of the Gough platform, analysis of the literature reveals that research into position control of this platform has not been carried out thoroughly. Moreover, most of the approaches have been directly imported from serial robotics. For instance, as the calculation of an accurate dynamic model of the platform is a challenging issue, some authors have proposed the use of local feedback controllers. Such devices control each link without considering the rest of the structure and are usually based on simple proportional-integral-derivative (PID) controllers. The simplest control approaches can be found in applications with heavy loads and slow motions. In ref. [29], for instance, a simple proportional controller is used to control actuators of a hydraulic platform, a PD controller is proposed in ref. [21] to control a 6 Prismatic-Spherical-Universal joints (PSU) prototype, and in ref. [39] a large fine-tuning platform based on the Gough platform is presented and controlled by means of a traditional servocontrol scheme. More sophisticated control approaches can be found when faster motion is to be achieved. In ref. [40] robust nonlinear PD-based control is proposed for reducing the tracking error, while in ref. [43] the gravitational term of the dynamic model is used with decoupled PD control to reduce positioning errors of a hydraulic platform. On the other hand, in ref. [35], the use of genetic algorithms to tune a task space PD controller is proposed in order to reduce tracking errors.

Although widely used in commercial platforms, local control approaches do not guarantee optimum performance when accuracy and speed are required. Hence, advanced control approaches have been proposed to increase dynamic performance. These controllers are based on dynamic models of the robot, using them to control all joints at the same time. One of the most popular approaches is the Computed Torque Control (CTC),[1,16] where the inverse dynamic model of the robot is used to compensate for the nonlinear dynamics of physical platform, thereby increasing the dynamic performance of the robot.

However, calculating an accurate inverse dynamic model is a difficult task, as errors arise in the process of identifying model parameters, simplifications are usually made, and some nonlinear physical phenomena, such as friction, are not considered. This has led some authors to propose robust schemes that guarantee the stability and performance of robots in the presence of uncertainty. For example, several authors[20,22,23,26] have suggested the use of a sliding-mode-based control to enhance the robustness of model-based approaches. In ref. [28], a computationally efficient and robust method is proposed based on the combination of the CTC approach with approximate dynamics and a compensation loop based on a H_∞ controller. Other authors[13,25] propose controllers based on the Lyapunov design approach, ensuring, by design, stability in the presence of uncertainty.

It is clear that the control of the Gough platform is still a challenging issue and an open field for research. Advanced control approaches require dynamic models that are difficult to derive and have to be as accurate as possible. In addition, as it is difficult to measure tool center point (TCP) coordinates directly, a kinematic model has to be used to estimate the values of these coordinates in terms of measurable variables, i.e., ones associated with actuated joints. Hence, if the kinematic model is not sufficiently accurate, estimation errors will arise decreasing the performance of the model-based controller.

An interesting approach to minimize the effect of parameter uncertainty is the use of extra sensors in the non-actuated joints of the mechanism, as proposed by several authors, including Merlet,[31] Parenti-Castelli and Di Gregorio,[36] Baron and Angeles,[4] Marquet *et al.*[30] and Bauma *et al.*[5] In general, the introduction of extra passive sensors in the structure of the mechanism can be difficult and increases costs. However, the use of sensors in certain specific non-actuated joints may reduce positioning errors, make the controller more robust against uncertainties in model parameters, and, with a proper selection, reduce the computational cost of the model. Thus, as shown in the previously cited papers, the benefits may outweigh the drawbacks.

In the current paper, exploiting the idea of using redundant sensor data in the control loop, a novel control approach, the Extended CTC (Extended CTC), is introduced. This control scheme, based on the previous work of the authors,[8,44] handles not only the position and velocity data of the

https://doi.org/10.1017/S0263574712000185 Published online by Cambridge University Press

actuators but also those provided by the extra sensors. This redundant information is processed by an inverse dynamic model defined in terms of both active joints and some sensorized non-actuated joints. This way the proposed approach has the advantages of the model-based approaches and lessens the model parameter identification problem, as it increases robustness against model parameter uncertainties. In order to demonstrate the effectiveness of the proposed Extended CTC approach, it is applied to the Gough platform and the results are compared with those obtained with the traditional CTC approach.

The rest of the paper is organized as follows. In Section 2 the Extended CTC concept is presented. Section 3 describes the methodology to calculate the redundant dynamic model of the Gough platform for a given passive joint sensor configuration. The redundant model obtained is validated in Section 4, and in Section 5, it is used to implement the Extended CTC approach in a set of simulations. Finally, in Section 6 the most important ideas are summarized.

2. Extended CTC Approach

It is well known that advanced control techniques are required to fully exploit the advantages of parallel robots for handling heavy loads and achieving high speed and accuracy. For that purpose, an accurate dynamic model is required. However, the calculation and identification of such models is not trivial, and simplifications are usually made.

In the classical CTC approach, the inverse dynamic model of the robot is used to linearize and decouple the nonlinear dynamics of the robot. Specifically, if the model were to be perfect, the nonlinear compensation feedback loop and the robot could be considered as a set of independent double integrators, one for each controlled variable. Hence, the linearized system could easily be controlled using a PD controller.

On the other hand, assuming that the model has inaccuracies, the decoupling and compensation are not perfect. In this case, the nonlinear compensation feedback loop and the robot model can be considered as the sum of a double integrator and a disturbance for each controlled variable. Further, the deviation in the kinematic parameters causes tool center point (TCP) positioning errors. Although in serial robotics kinematic parameters can be properly identified and tuned using calibration procedures, in general these procedures are not applicable in parallel robots.

The Extended CTC control approach is based on a redundant dynamic model so that information from some strategic non-actuated joints of the mechanism is passed to the controller. This way, as the controller is fed with more information, errors due to phenomena not modelled and uncertainties have less effect in the performance of the controller, as better estimations can be made if sensor data are sufficiently accurate.

In order to apply the Extended CTC approach, proper dynamic and kinematic models are needed. For this, the dynamic and kinematic models have to use real data from passive joints. That is, as the sensorized non-actuated joint positions and velocities are measured, they will be considered as knowns.

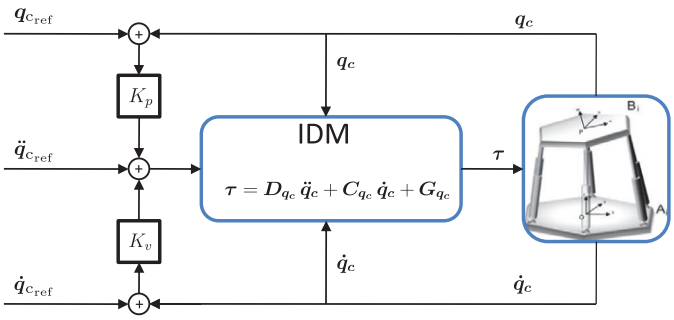


Fig. 2. (Colour online) Extended CTC in joint space (JS).

In order to introduce the Extended CTC control law, the following variables are defined. Let $\mathbf{q_a}$ be the active joint variables, $\mathbf{q_s}$ be the non-actuated sensorized joint variables, and $\mathbf{q_p}$ be the passive joint variables, which are not sensorized. The set of all non-actuated variables is then written as $\mathbf{q_{na}} = [\,\mathbf{q_s}^T\ \mathbf{q_p}^T\,]^T$ and, in order to group the measurable data, i.e., the joint variables that are sensorized, the *control coordinates'* vector is defined as $\mathbf{q_c} = [\,\mathbf{q_a}^T\ \mathbf{q_s}^T\,]^T$.

Thus, if the Extended CTC approach is defined in the joint space (JS) (Fig. 2), the control law,

$$\begin{aligned}\boldsymbol{\tau} = {} & \mathbf{D_{q_c}}(\mathbf{q_c}, \mathbf{q_p}, \mathbf{x})\ \left(\ddot{\mathbf{q}}_{\mathbf{c_{ref}}} + \mathbf{K_v}\,\dot{\mathbf{e}}_{\mathbf{q_c}} + \mathbf{K_p}\,\mathbf{e}_{\mathbf{q_c}}\right) \\ & + \mathbf{C_{q_c}}(\mathbf{q_c}, \mathbf{q_p}, \mathbf{x}, \dot{\mathbf{q}}_\mathbf{c}, \dot{\mathbf{q}}_\mathbf{p}, \dot{\mathbf{x}})\,\dot{\mathbf{q}}_\mathbf{c} + \mathbf{G_{q_c}}(\mathbf{q_c}, \mathbf{q_p}, \mathbf{x}),\end{aligned} \tag{1}$$

where $\mathbf{K_p}$ and $\mathbf{K_v}$ are the position and velocity matrix gains, respectively, $\mathbf{e_{q_c}} = \mathbf{q_{c_{ref}}} - \mathbf{q_c}$ is the tracking error and $\dot{\mathbf{e}}_{\mathbf{q_c}}$ is its time derivative, $\mathbf{q_{c_{ref}}}$ is the reference of the control coordinates, $\mathbf{D_{q_c}}$ is the inertia matrix, $\mathbf{C_{q_c}}$ is the Coriolis matrix, $\mathbf{G_{q_c}}$ is the gravity vector, $\boldsymbol{\tau}$ is the torques/forces associated with the active joints of the robot, and $\mathbf{x}$ is the task coordinate vector.

As can be seen in Eq. (1), all measurable variables, grouped into the control coordinates' vector, are explicitly used in the dynamic model to estimate the nonmeasurable data, i.e., the position and velocity of the end effector ($\mathbf{x}$, $\dot{\mathbf{x}}$) and the passive joint variables ($\mathbf{q_p}$, $\dot{\mathbf{q}}_\mathbf{p}$). As there may be redundancy in control coordinates, the Inertia and Coriolis matrices are not, in general, square and they project the redundant data into the actuated space in which the actuator forces $\boldsymbol{\tau}$ are defined.

On the other hand, if the Extended CTC approach is defined in the task space (TS) (Fig. 3), then the control coordinates will be the task coordinates $\mathbf{x}$. However, as these coordinates cannot be directly measured, they are estimated from all the measurable variables, i.e., the control coordinates $\mathbf{q_c}$. Accordingly, the dynamic model used to implement the Extended CTC in Eq. (1) will have to be projected into the task space using kinematic relations. This way, with the Extended CTC defined in the task space,

$$\begin{aligned}\tau = {} & \mathbf{D_x}(\mathbf{q_c}, \mathbf{q_p}, \mathbf{x})\ \left(\ddot{\mathbf{x}}_{\mathbf{ref}} + \mathbf{K_v}\,\dot{\mathbf{e}}_\mathbf{x} + \mathbf{K_p}\,\mathbf{e}_\mathbf{x}\right) \\ & + \mathbf{C_x}(\mathbf{q_c}, \mathbf{q_p}, \mathbf{x}, \dot{\mathbf{q}}_\mathbf{c}, \dot{\mathbf{q}}_\mathbf{p}, \dot{\mathbf{x}})\,\dot{\mathbf{x}} + \mathbf{G_x}(\mathbf{q_c}, \mathbf{q_p}, \mathbf{x}),\end{aligned} \tag{2}$$

https://doi.org/10.1017/S0263574712000185 Published online by Cambridge University Press

Table I. Parameters of the Gough platform.

Body	Length	Mass	Inertia	Center of mass
Cylinder	l_{i_1}	m_{i_1}	I_{i_1}	$l_{c_{i1}}$
Rod	l_{i_2}	m_{i_2}	I_{i_2}	$l_{c_{i2}}$
Mobile platform	–	m_p	I_p	$P(x, y, z)$
Load	–	m_c	I_c	$P(x, y, z)$

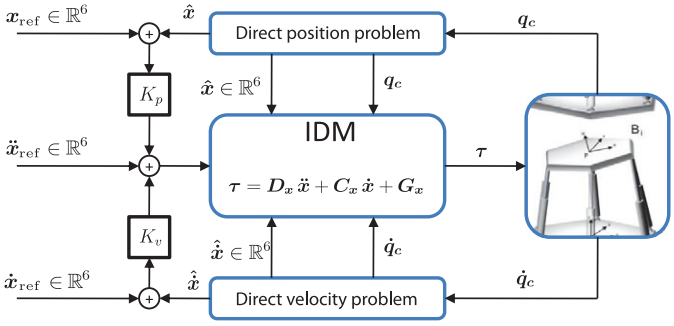


Fig. 3. (Colour online) Extended CTC in task space (TS).

where $\mathbf{e_x} = \mathbf{x_{ref}} - \mathbf{x}$ is the estimated tracking error, $\mathbf{D_x}$ is the inertia matrix, $\mathbf{C_x}$ is the Coriolis matrix, $\mathbf{G_x}$ is the gravity vector, and $\boldsymbol{\tau}$ is the force associated with active joints. In this case, the measurable data are introduced implicitly in the model and used to provide better estimates of nonmeasurable variables.

3. Redundant Dynamic Modelling of the Gough Platform

The Gough platform is composed of a mobile platform (MP) connected to a fixed base platform by six extensible $U\underline{P}S$ serial chain limbs. Let $O(x, y, z)$ be the fixed reference frame of the system attached to the base platform and $P(u, v, w)$ is the moving frame attached to the center of mass of the mobile platform where the TCP is also located, as shown in Fig. 4.

Each universal joint U connects its associated limb to the base platform at points $\mathbf{A_i}$, $i = 1, \ldots 6$, whose position in the fixed reference frame is given by the vector $\mathbf{a_i}$. The limb is actuated by means of a prismatic joint $\underline{P}$ with a variable length l_i. This linear motion is achieved by relative movement between a cylinder and a rod, characterized by lengths l_{i_1} and l_{i_2}, respectively (Fig. 5). A spherical joint S connects each of the limbs to the mobile platform at points $\mathbf{B_i}$, $i = 1, \ldots 6$, whose position in the moving frame is given by vector $\mathbf{d_i}$. The parameters of the mechanism are summarized in Table I and illustrated in Figs. 4 and 5.

In addition, the following variables and coordinates are defined. Let $\mathbf{p_x} = [\, x\ y\ z\,]^T$ be the cartesian position of point $\mathbf{P}$ where the TCP is located. The orientation of the moving platform is given by the rotation matrix $R(\alpha, \beta, \gamma)$ that relates the fixed frame of reference $O(x, y, z)$ to the moving frame whose origin is point $\mathbf{P}$. Then the location of the TCP is given by the output or task coordinates $\mathbf{x} = [\, x\ y\ z\ \alpha\ \beta\ \gamma\,]^T$.

The active joint variable vector is defined as $\mathbf{q_a} = [\, l_1 \ldots l_6\,]^T$ and the non-actuated joint variable vector as $\mathbf{q_{na}} = [\, \boldsymbol{\theta}^T\ \boldsymbol{\varphi}^T\,]^T_{12\times1}$, where $\boldsymbol{\theta} = [\, \theta_1 \ldots \theta_6\,]^T$ and $\boldsymbol{\varphi} = [\, \varphi_1 \ldots \varphi_6\,]^T$ are the non-actuated joint variables shown in Fig. 6. Thus, the vector that groups all joint variables is defined as $\mathbf{q} = [\, \mathbf{q_a}^T\ \mathbf{q_{na}}^T\,]^T_{18\times1}$.

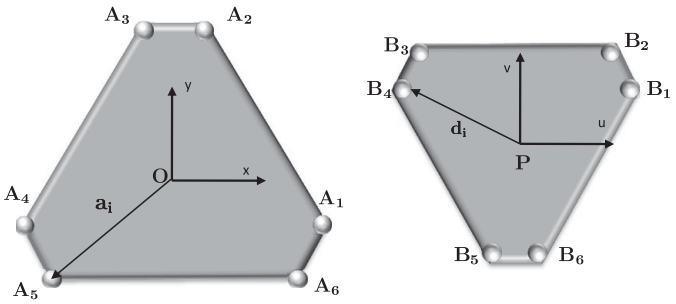


Fig. 4. Schematic of the base and mobile platform.

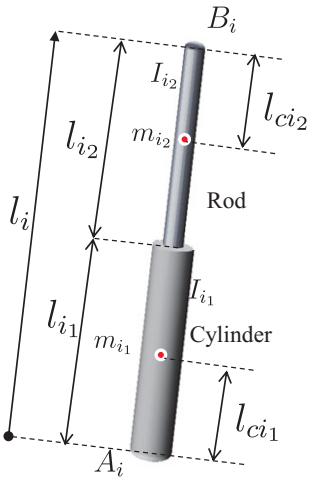


Fig. 5. (Colour online) Schematic of the limbs: cylinder and rod.

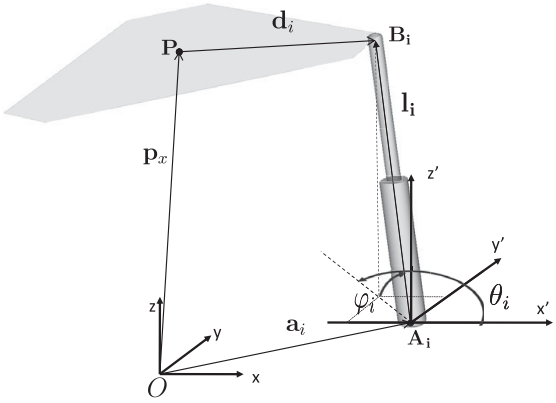


Fig. 6. Loop closure equation of kinematic chain i.

In order to apply the Extended CTC approach, a redundant dynamic model of the Gough platform is required. This model allows the redundant information from extra sensors and actuators to be used in the control law, reducing the need to estimate some of the model variables. In this section, the procedure to calculate such a dynamic model is detailed. This procedure is based on three important ideas.

First, the dynamic model will be defined using the information provided by all measurable joint variables, i.e., *control coordinates* vector $\mathbf{q_c} = [\, \mathbf{q_a}^T\ \mathbf{q_s}^T\,]^T \in \mathbb{R}^{n_c}$, with

https://doi.org/10.1017/S0263574712000185 Published online by Cambridge University Press

$n_c = (6, 18)$. Note that the set of control coordinates will vary depending on the number of sensorized non-actuated joints $\mathbf{q_s}$. Thus, in order to specify the measurable variables for a given sensor configuration, a *selection vector* $\mathbf{I_c}$ is defined. This vector contains the indices of joint variables that are sensorized, so that $\mathbf{q_c} = [\mathbf{q}]_{\mathbf{I_c}}$. As will be seen later, the use of the selection vector $\mathbf{I_c}$ will allow a reconfigurable dynamic model to be calculated for different sensor configurations.

Second, the Lagrangian Formulation is used to derive the dynamic model in terms of $\mathbf{q_c}$. This approach avoids the calculation of internal forces of the mechanism, and it allows the designer to choose the most suitable generalized coordinates for the design of the dynamic model. Thus, it is suitable for expressing the dynamic model in terms of a redundant set of coordinates, as the Extended CTC approach requires.

Third, the procedure detailed in this section considers the mechanism as a two-part subsystem composed of the serial kinematic chains and the moving platform.[6] This way, the Lagrangian of the mechanism is constructed from the contribution of the Lagrangian of the two subsystems. In addition, the equations of each subsystem will be expressed in natural coordinate systems. Therefore, the mobile platform equations will be expressed in terms of the task coordinates $\mathbf{x}$, while the limbs will be expressed in terms of the generalized joint coordinates $\mathbf{q}$ that group actuated and non-actuated joints.

Next, the guidelines for the calculation of the kinematic and dynamic model of the Gough platform in terms of the redundant control coordinates $\mathbf{q_c}$ will be detailed. In this procedure, the masses of the bodies will be considered to be concentrated in their center of mass and friction will be neglected, as will the mass and inertia of extra sensors.

3.1. Loop closure equations

The six vector loop closure equations that define the constraints of the mechanism are shown in Fig. 6, where each vector $\mathbf{l}_i$ is defined in terms of joint variables associated with each of the serial chains $\mathbf{q_i} = [\, l_i \;\; \theta_i \;\; \varphi_i \,]^T$.

Thus, the vector loop closure equation associated with kinematic chain i with $i = 1, \ldots 6$ is

$$\mathbf{a_i} + \mathbf{l_i} - \mathbf{p_x} - \mathbf{R}(\alpha, \beta, \gamma)\, \mathbf{d_i} = \Gamma_\mathbf{i}(\mathbf{x}, \mathbf{q_i}) = \mathbf{0}_{3\times 1}, \qquad (3)$$

where $[\mathbf{d_i}]_{3\times 1}$ is a constant vector that defines the geometry of the mobile platform in the moving frame, $[\mathbf{a_i}]_{3\times 1}$ is the position vector of points $\mathbf{A_i}$ with respect to the fixed frame, and $\mathbf{R}(\alpha, \beta, \gamma)$ is the rotation matrix that defines the orientation of the moving platform with respect to the fixed frame. If the Euler Roll-Pitch-Yaw (*RPY*) notation is used,

$$\mathbf{R} = \begin{bmatrix} c\gamma\, c\beta & c\gamma\, s\beta\, s\alpha - s\gamma\, c\alpha & s\gamma\, s\alpha + c\gamma\, s\beta\, c\alpha \\ s\gamma\, c\beta & c\gamma\, c\alpha + s\gamma\, s\beta\, s\alpha & s\gamma\, s\beta\, c\alpha - c\gamma s\alpha \\ -s\beta & c\beta\, s\alpha & c\beta\, c\alpha \end{bmatrix},$$

where c and s stand for the trigonometric functions cosine and sine, respectively.

Finally, the vector associated with limb i, $\mathbf{l_i} = \overrightarrow{A_i B_i}$ can be expressed in terms of joint variables associated with the ith limb, $\mathbf{q_i}$

$$\mathbf{l_i} = \left[l_i \;\cos\theta_i \cos\varphi_i \;\; l_i \;\sin\theta_i \cos\varphi_i \;\; l_i \;\sin\varphi_i \right]^T, \qquad (4)$$

where $\|\mathbf{l_i}\| = l_i$.

Combining the loop closure equations of all kinematic chains, the constraint equation set of the mechanism is

$$[\Gamma_\mathbf{i}(\mathbf{x}, \mathbf{q_i})]_{i=1,\ldots 6} = \Gamma(\mathbf{x}, \mathbf{q}) = \mathbf{0}_{18\times 1}. \qquad (5)$$

3.2. Inverse Kinematic Problem

For the Inverse Kinematic Model the values of the active joint variables $\mathbf{q_a}$ can be expressed in terms of a given set of task coordinates $\mathbf{x}$. Thus, if the TCP pose $\mathbf{x}$ is known, the cartesian position of points $\mathbf{B_i} = \mathbf{p_x} + \mathbf{R}\,\mathbf{d_i}$ can be calculated. Thereby, imposing $l_i^2 = ||\mathbf{l_i}||^2$ on the vectorial loop closure equation (3),

$$\begin{aligned} l_i^2 &= \mathbf{l_i}^T \mathbf{l_i} \\ &= [\mathbf{p_x} - \mathbf{a_i} + \mathbf{R}(\alpha, \beta, \gamma)\, \mathbf{d_i}]^T \;[\mathbf{p_x} - \mathbf{a_i} + \mathbf{R}(\alpha, \beta, \gamma)\, \mathbf{d_i}], \end{aligned} \qquad (6)$$

where the values of active joints $l_i = q_{a_i}$, $i = 1 \ldots 6$ can be calculated.

3.3. Non-actuated joints variables value

The values of each of the non-actuated joint variables $\mathbf{q_{na}} = [\, \theta^T \;\; \varphi^T \,]^T$ can be expressed in terms of the active joint variables $\mathbf{q_a}$ and the task coordinates $\mathbf{x}$. If Eqs. (3) and (4) are combined,

$$\mathbf{l_i} = \mathbf{p_x} - \mathbf{a_i} + R(\alpha, \beta, \gamma)\, \mathbf{d_i} = \begin{bmatrix} l_i & \cos\theta_i & \cos\varphi_i \\ l_i & \sin\theta_i & \cos\varphi_i \\ & l_i \sin\varphi_i & \end{bmatrix}, \qquad (7)$$

using the vectorial equation,

$$\begin{cases} \varphi_i = atan2\left(l_{iz}, \sqrt{l_{ix}^2 + l_{iy}^2}\right), \\ \theta_i = atan2\left(l_{iy}, l_{ix}\right) \end{cases} \qquad (8)$$

where l_{ix}, l_{iy}, and l_{iz} are the x, y, and z coordinates of vector $\mathbf{l_i} = \mathbf{p_x} - \mathbf{a_i} + R\,\mathbf{d_i}$ and $atan2$ is the four-quadrant inverse tangent. Note that φ_i always lies in the first quadrant.

3.4. Direct Kinematic Problem

The Direct Kinematic Problem (DKP) calculates the value of the pose of the TCP $\mathbf{x}$ in terms of all measurable joint variables. It is well known that using only the six active joints as inputs, the DKP of the Gough platform can have up to 40 different solutions. Thus, iterative methods are usually implemented to solve nonlinear equations.

In previous studies, sensor redundancy has been applied to solve this issue. Some authors have focused on reducing the

https://doi.org/10.1017/S0263574712000185 Published online by Cambridge University Press

computational time required to solve the DKP by determining the set of extra sensors necessary to obtain a closed-form solution.[31,36] However, because of advances in computer technology, this issue is not as critical as before. Other authors have proposed using the extra information to obtain a better or more robust estimate of the location of the TCP.[4] In this section, a generic procedure to calculate $\mathbf{x}$ in terms of the set of measurable joints $\mathbf{q_c}$ is detailed. This approach is based on the iterative minimization of the loop closure equation functions and has two advantages over previously proposed methods: first, as it is based on the use of the selection vector $\mathbf{I_c}$, it is defined for any set of $\mathbf{q_c}$; and second, when parameter uncertainties arise, an attempt is made to minimize the closure equations errors using all the available information, resulting in a more accurate estimation, provided that the initial guess is sufficiently close.

For that purpose, the equations that relate different joint coordinates grouped in $\mathbf{q}$ and task coordinates $\mathbf{x}$ are calculated. First, the equations that relate each of the active joints $\mathbf{q_a} = [l_i]_{i=1,\dots 6}$ and the task coordinates are obtained from Eq. (6),

$$\left[||\mathbf{l_i}||^2 - l_i^2\right]_{i=1\dots 6} = \mathbf{0}_{6\times 1}. \tag{9}$$

The equations that relate each of the non-actuated joints $\mathbf{q_{na}}$ and the task coordinates $\mathbf{x}$ are obtained from Eq. (8),

$$\begin{aligned} \left[l_{ix}\ \tan\theta_i - l_{iy}\right]_{i=1\dots 6} &= \mathbf{0}_{6\times 1}, \\ \left[\sqrt{l_{ix}^2 + l_{iy}^2}\ \tan\varphi_i - l_{iz}\right]_{i=1\dots 6} &= \mathbf{0}_{6\times 1}. \end{aligned} \tag{10}$$

Thus, combining Eqs. (9) and (10),

$$\mathbf{F} = \begin{bmatrix} \left[||\mathbf{l_i}|| - l_i^2\right]_{i=1\dots 6} \\ \left[l_{ix}\ \tan\theta_i - l_{iy}\right]_{i=1\dots 6} \\ \left[\sqrt{l_{ix}^2 + l_{iy}^2}\ \tan\varphi_i - l_{iz}\right]_{i=1\dots 6} \end{bmatrix} = \mathbf{0}_{18\times 1}, \tag{11}$$

which defines the set of equations that relates each of the joint variables in $\mathbf{q}$ and the task coordinates $\mathbf{x}$.

Note that each of the equations in the system of Eq. (11) is associated with a single joint variable. Thus, the selection vector $\mathbf{I_c}$ can be used to extract the equations of $\mathbf{F}$, which are associated with the control coordinates $\mathbf{q_c}$,

$$\mathbf{F}_c = [\mathbf{F}]_{\mathbf{I_c}} = \mathbf{0} \tag{12}$$

that, if the control coordinates $\mathbf{q_c}$ include redundant information, define an over-determined system.

The system of Eq. (12) can be solved using an appropriate iterative algorithm, obtaining the value of the TCP location $\mathbf{x}$. Note that in this approach the extra information is directly used to estimate $\mathbf{x}$. Thus, if kinematic uncertainties arise, this extra data are used to minimize the estimation error, as the algorithm tries to reduce the residuals in all the equations, one for each measured variable.

3.5. Velocity problem

The Gough platform is a spatial platform whose orientation is determined using *RPY* Euler angles $\boldsymbol{\psi} = [\,\alpha\ \beta\ \gamma\,]^T$. This way the location of the TCP is defined as $\mathbf{x} = [\,x\ y\ z\ \alpha\ \beta\ \gamma\,]^T$.

However, the direct derivation of this vector with respect to time $\dot{\mathbf{x}}$ only has physical meaning for the translational terms of $\mathbf{x}$.[2] This is a key issue when dealing with spatial platforms, as the equations of motion of rigid bodies are defined in terms of the angular velocity and acceleration of the body, and not in terms of the Euler angles. Thus, in order to calculate the dynamic model of the mechanism, the relation between the time derivatives of the Euler angles $\dot{\boldsymbol{\psi}} = [\,\dot\alpha\ \dot\beta\ \dot\gamma\,]^T$ and the angular velocity of the moving frame with respect to the fixed frame, $\omega = [\,\omega_x\ \omega_y\ \omega_z\,]^T$, is needed.

This relationship is given by the following expression:[19]

$$\boldsymbol{\omega} = \mathbf{R}\,\mathbf{E}\,\dot{\boldsymbol{\psi}}, \tag{13}$$

where if RPY Euler angles are considered, then

$$\mathbf{E} = \begin{bmatrix} 1 & 0 & -\sin\beta \\ 0 & \cos\alpha & \cos\beta\ \sin\alpha \\ 0 & -\sin\alpha & \cos\beta\ \cos\alpha \end{bmatrix}.$$

Accordingly, the velocity vector, $\mathbf{v} = [\,\dot{\mathbf{p}}_{\mathbf{x}}^T\ \boldsymbol{\omega}^T\,]^T$, can be written as

$$\mathbf{v} = \begin{bmatrix} \mathbf{I} & \mathbf{0} \\ \mathbf{0} & \mathbf{R}\,\mathbf{E} \end{bmatrix} \dot{\mathbf{x}} = \mathbf{T}_{\mathbf{R}}\,\dot{\mathbf{x}}. \tag{14}$$

With these definitions, the velocity equations can then be derived.

Link Jacobian matrices $\mathbf{J_i}$. The link Jacobian matrices define the velocity problem of the mechanism and are calculated by differentiating the loop closure equations defined in Eq. (3) with respect to time. Thus,

$$\dot{\mathbf{l}}_{\mathbf{i}} = \dot{\mathbf{p}}_{\mathbf{x}} + \dot{\mathbf{R}}\,\mathbf{d_i}. \tag{15}$$

Let $\mathbf{a}$ and $\mathbf{b}$ be two vectors, then $\tilde{\mathbf{a}}\mathbf{b} = \mathbf{a}\times\mathbf{b}$, where $\times$ is the cross-product operation. Then,

$$\dot{\mathbf{l}}_{\mathbf{i}} = \dot{\mathbf{p}}_{\mathbf{x}} + \boldsymbol{\omega}\times\mathbf{R}\,\mathbf{d_i} = \dot{\mathbf{p}}_{\mathbf{x}} - \mathbf{R}\,\mathbf{d_i}\times\boldsymbol{\omega}, \tag{16}$$

where $\mathbf{R}\,\mathbf{d_i} = \mathbf{d_i^O}$ is the projection of constant vector $\mathbf{d_i}$ in the fixed frame, which satisfies $\tilde{\mathbf{d}}_{\mathbf{i}}^{\mathbf{O}} = \mathbf{R}\,\tilde{\mathbf{d}}_{\mathbf{i}}\,\mathbf{R}^T$. Then

$$\dot{\mathbf{l}}_{\mathbf{i}} = \dot{\mathbf{p}}_{\mathbf{x}} - \mathbf{R}\,\tilde{\mathbf{d}}_{\mathbf{i}}\,\mathbf{R}^T\,\boldsymbol{\omega} = \left[\,\mathbf{I}_{3\times 3}\ -\mathbf{R}\,\tilde{\mathbf{d}}_{\mathbf{i}}\,\mathbf{R}^T\,\right]\mathbf{v}. \tag{17}$$

Using Eq. (14), $\mathbf{v}$ can be replaced by $\dot{\mathbf{x}}$, giving

$$\dot{\mathbf{l}}_{\mathbf{i}} = \left(\left[\,\mathbf{I}_{3\times 3}\ -\mathbf{R}\,\tilde{\mathbf{d}}_{\mathbf{i}}\,\mathbf{R}^T\,\right]\mathbf{T}_{\mathbf{R}}\right)\dot{\mathbf{x}} = \mathbf{J}_{\mathbf{x_i}}\,\dot{\mathbf{x}}. \tag{18}$$

Differentiating Eq. (4) with respect to time,

$$\begin{aligned} \dot{\mathbf{l}}_{\mathbf{i}} &= -\begin{bmatrix} -c\,\varphi_i\,c\,\theta_i & l_i\,c\,\varphi_i\,s\,\theta_i & l_i\,c\,\theta_i\,s\,\varphi_i \\ -c\,\varphi_i\,s\,\theta_i & -l_i\,c\,\varphi_i\,c\,\theta_i & l_i\,s\,\varphi_i\,s\,\theta_i \\ -s\,\varphi_i & 0 & -l_i\,c\,\varphi_i \end{bmatrix}\dot{\mathbf{q}}_{\mathbf{i}} \\ &= -\underbrace{\mathbf{J}_{\mathbf{q_i}}}_{3\times 3}\,\dot{\mathbf{q}}_{\mathbf{i}}, \end{aligned} \tag{19}$$

https://doi.org/10.1017/S0263574712000185 Published online by Cambridge University Press

where $\dot{\mathbf{q}}_\mathbf{i} = [\,\dot{l}_i\ \dot{\theta}_i\ \dot{\varphi}_i\,]^T$.

Thus, the link Jacobian matrix associated with the serial chain i being $\mathbf{J_i}$,

$$-\mathbf{J}_{\mathbf{q_i}}\,\dot{\mathbf{q}}_\mathbf{i} = \mathbf{J}_{\mathbf{x_i}}\,\dot{\mathbf{x}} \rightarrow \dot{\mathbf{q}}_\mathbf{i} = -\underbrace{\mathbf{J}_{\mathbf{q_i}}{}^{-1}}_{3\times3}\,\underbrace{\mathbf{J}_{\mathbf{x_i}}}_{3\times6}\,\dot{\mathbf{x}} = \underbrace{\mathbf{J_i}}_{3\times6}\,\dot{\mathbf{x}}. \tag{20}$$

Using the six-link Jacobian matrices of the Gough platform, the other velocity equations can be obtained as follows.

Joint variables Jacobian $\mathbf{J_q}$. This relates the joint velocities $\dot{\mathbf{q}}_\mathbf{a}$, $\dot{\mathbf{q}}_\mathbf{na}$ to the derivatives of the task coordinates $\mathbf{x}$.

Let $[\mathbf{A}]_i$ define the row operator that extracts the ith row of a matrix $\mathbf{A}$. Then the joint variables Jacobian $\mathbf{J_q}$ is defined by

$$\dot{\mathbf{q}} = \underbrace{\mathbf{J_q}}_{18\times6}\,\dot{\mathbf{x}} = \begin{bmatrix}\mathbf{J}_{\mathbf{q_a}}\\ \mathbf{J}_{\mathbf{q_{na}}}\end{bmatrix}\dot{\mathbf{x}}, \tag{21}$$

where

$$\mathbf{J}_{\mathbf{q_a}} = \left[\,[\mathbf{J_1}]_1^T\ \ldots\ [\mathbf{J_6}]_1^T\,\right]^T,$$
$$\mathbf{J}_{\mathbf{q_{na}}} = \left[\,[\mathbf{J_1}]_2^T\ \ldots\ [\mathbf{J_6}]_2^T\ [\mathbf{J_1}]_3^T\ \ldots\ [\mathbf{J_6}]_3^T\,\right]^T.$$

Platform Jacobian $\mathbf{J_p}$. This relates the derivatives of the control coordinates $\dot{\mathbf{q}}_\mathbf{c}$ to the derivatives of the task coordinates $\dot{\mathbf{x}}$,

$$\dot{\mathbf{x}} = \mathbf{J_p}\,\dot{\mathbf{q}}_\mathbf{c} = \mathbf{J}_{\mathbf{q_c}}{}^{\dagger}\,\dot{\mathbf{q}}_\mathbf{c}, \tag{22}$$

where $\mathbf{J}_{\mathbf{q_c}}{}^{\dagger}$ is the Moore–Penrose generalized pseudoinverse of the Jacobian matrix associated with the control coordinates, $\mathbf{J_c} = [\mathbf{J_q}]_{\mathbf{I_c}}$.

On the other hand, the rows corresponding to the non-actuated and non-sensorized joint variables $\mathbf{q_p}$ are used to calculate the Jacobian of the strictly passive joints, $\dot{\mathbf{q}}_\mathbf{p} = \mathbf{J}_{\mathbf{q_p}}\,\dot{\mathbf{x}}$.

$\mathbf{T}$ *and* $\mathbf{T_q}$ *matrices.* These matrices are defined using the previously defined Jacobians, and are used to project the dynamic model into the actuator and control coordinate joint variable spaces,

$$\dot{\mathbf{q}} = \begin{bmatrix}\mathbf{I_3}\\ \mathbf{J}_{\mathbf{q_{na}}}\,\mathbf{J}_{\mathbf{q_a}}{}^{-1}\end{bmatrix}^T\dot{\mathbf{q}}_\mathbf{a} = \mathbf{T}\,\dot{\mathbf{q}}_\mathbf{a}, \tag{23}$$

$$\dot{\mathbf{q}} = \underbrace{\mathbf{T_q}}_{18\times n_c}\,\dot{\mathbf{q}}_\mathbf{c},\ \left[\mathbf{T_q}\right]_i = \begin{cases}\mathbf{e_j}^T,\ q_i = q_{c_j} \in \mathbf{q_c}\\ \left[\mathbf{J}_{\mathbf{q_p}}\,\mathbf{J_p}\right]_k,\ q_i = q_{p_k} \in \mathbf{q_p}\end{cases}, \tag{24}$$

where

$$\left[\mathbf{e_j}\right]_i = \begin{cases}1, & i = j\\ 0, & i \neq j\end{cases}.$$

If $\mathbf{q_c} = \mathbf{q_a}$, then $\mathbf{T_q} = \mathbf{T}$.

3.6. Acceleration problem

Acceleration equations are calculated by differentiating velocity equations with respect to time. Thus, differentiating Eq. (20) with respect to time, the acceleration equations for each serial chain i can be written as

$$\begin{aligned}\ddot{\mathbf{q}}_\mathbf{i} &= \mathbf{J}_{\mathbf{q_i}}{}^{-1}\,\mathbf{J}_{\mathbf{x_i}}\,\ddot{\mathbf{x}} - \mathbf{J}_{\mathbf{q_i}}{}^{-1}\left(\dot{\mathbf{J}}_{\mathbf{x_i}} + \dot{\mathbf{J}}_{\mathbf{q_i}}\,\mathbf{J_i}\right)\dot{\mathbf{x}},\\ \ddot{\mathbf{q}}_\mathbf{i} &= \mathbf{J_i}\,\ddot{\mathbf{x}} + \dot{\mathbf{J}}_\mathbf{i}\,\dot{\mathbf{x}}.\end{aligned} \tag{25}$$

Using this expression, the other acceleration equations can be obtained. Differentiating Eq. (21), the Jacobian associated with the acceleration of the joint variables $\dot{\mathbf{J}}_\mathbf{q}$ is defined by

$$\begin{aligned}\ddot{\mathbf{q}} &= \begin{bmatrix}\mathbf{J}_{\mathbf{q_a}}\\ \mathbf{J}_{\mathbf{q_{na}}}\end{bmatrix}\ddot{\mathbf{x}} + \begin{bmatrix}\dot{\mathbf{J}}_{\mathbf{q_a}}\\ \dot{\mathbf{J}}_{\mathbf{q_{na}}}\end{bmatrix}\dot{\mathbf{x}},\\ \ddot{\mathbf{q}} &= \mathbf{J_q}\,\ddot{\mathbf{x}} + \dot{\mathbf{J}}_\mathbf{q}\,\dot{\mathbf{x}}.\end{aligned} \tag{26}$$

Similarly, the Jacobian associated with the acceleration of the platform $\dot{\mathbf{J}}_\mathbf{p}$ is obtained following the same procedure described for the platform Jacobian, yielding

$$\ddot{\mathbf{x}} = \mathbf{J_p}\,\ddot{\mathbf{q}}_\mathbf{c} + \dot{\mathbf{J}}_\mathbf{p}\,\dot{\mathbf{q}}_\mathbf{c} = \mathbf{J}_{\mathbf{q_c}}{}^{\dagger}\,\ddot{\mathbf{q}}_\mathbf{c} - \mathbf{J_p}\,\dot{\mathbf{J}}_{\mathbf{q_c}}\,\mathbf{J_p}\,\dot{\mathbf{q}}_\mathbf{c}. \tag{27}$$

Finally, considering the time derivative of matrix $\mathbf{T_q}$,

$$\ddot{\mathbf{q}} = \underbrace{\mathbf{T_q}}_{18\times n_c}\,\ddot{\mathbf{q}}_\mathbf{c} + \underbrace{\dot{\mathbf{T}}_\mathbf{q}}_{18\times n_c}\,\dot{\mathbf{q}}_\mathbf{c}. \tag{28}$$

3.7. Lagrangian equation

As stated in the introduction to this section, the proposed method considers that the Gough platform is composed of two subsystems, the moving platform and the limbs. Thus, the Lagrangian of the robot can be calculated as the sum of the contribution of the Lagrangian of each subsystem, which will be calculated in terms of its natural coordinates. That is, the mobile platform equations will be defined in terms of the task coordinates $\mathbf{x}$, while the limbs will be defined in terms of the joint coordinates $\mathbf{q}$.

Mobile platform. The kinetic K_{MP} and potential U_{MP} energies of the moving platform are calculated as follows:

$$\begin{aligned}K_{MP} &= \tfrac{1}{2}\,\dot{\mathbf{x}}^T\,\mathbf{T_R}^T\begin{bmatrix}\left(m_p + m_c\right)\mathbf{I}_3 & \mathbf{0}_3\\ \mathbf{0}_3 & \mathbf{I_c} + \mathbf{I_p}\end{bmatrix}\mathbf{T_R}\,\dot{\mathbf{x}}\\ &= \tfrac{1}{2}\,\dot{\mathbf{x}}^T\,\underbrace{\mathbf{M_x(x)}}_{6\times6}\,\dot{\mathbf{x}},\end{aligned} \tag{29}$$

where $\mathbf{M_x(x)}$ is the inertia matrix of the moving platform, defined in terms of $\mathbf{x}$, and

$$U_{MP} = \left(m_p + m_c\right)g\,z, \tag{30}$$

where g is the gravity.

Limbs-cylinder. The six limbs that join the moving platform with the base platform are structurally identical. Each one can be considered as a polar 3-DOF serial robot (Fig. 5) and

https://doi.org/10.1017/S0263574712000185 Published online by Cambridge University Press

is constituted of two bodies, a cylinder and a rod, whose contribution to the Lagrangian has to be calculated.

The center of mass (CM) of the cylinder of the ith kinematic chain,

$$\mathbf{CM}_{i1} = \mathbf{a_i} + \begin{bmatrix} l_{ci_1} & \cos\theta_i & \cos\varphi_i \\ l_{ci_1} & \sin\theta_i & \cos\varphi_i \\ & l_{ci_1} & \sin\varphi_i \end{bmatrix}, \tag{31}$$

where $\mathbf{a_i}$ is constant.

Differentiating Eq. (31) with respect to time, the linear velocity of the CM, $\mathbf{v_{i1}}$, can be expressed as

$$\mathbf{v_{i1}} = \frac{\partial \mathbf{CM_{i1}}}{\partial \mathbf{q}}\,\dot{q} = \mathbf{E}_{\mathbf{v_{i1}}}\,\dot{q}, \tag{32}$$

where $\mathbf{E}_{\mathbf{v_{i1}}}$ is the Jacobian that relates the linear velocity of the CM to the derivatives of joint variables.

In order to calculate the angular velocity of the CM, $\boldsymbol{\omega_{i1}}$, a reference frame will be attached to the CM of the cylinder whose axes are defined in the directions of the principal inertia axes. This way the products of inertia of the centroidal inertia tensor $\mathbf{I_{i1}}$ will be null.

Projecting the angular velocity vectors $\dot{\theta}_\mathbf{i}$ and $\dot{\varphi}_\mathbf{i}$ in the centroidal reference frame attached to the body, the value of the angular velocity of the CM, $\boldsymbol{\omega_{i1}}$, can be calculated in terms of the velocities of joint variables,

$$\boldsymbol{\omega_{i1}} = \begin{bmatrix} \dot{\theta}_i\ \sin\varphi_i & -\dot{\varphi}_i\ \dot{\theta}_i\ \cos\varphi_i \end{bmatrix}^T. \tag{33}$$

Rearranging in terms of $\mathbf{q}$, the following expression can be obtained,

$$\boldsymbol{\omega_{i1}} = \mathbf{E}_{\boldsymbol{\omega}_{i1}}\,\dot{\mathbf{q}} \tag{34}$$

where $\mathbf{E}_{\boldsymbol{\omega}_{i1}}$ is the Jacobian matrix that relates the angular velocity to the derivatives of joint variables.

Expressions having been obtained for the velocities, the kinetic energy of the cylinder can be written as

$$\begin{aligned} K_{s_{i1}} &= \tfrac{1}{2}\,\dot{\mathbf{q}}^T \left(m_{i1}\,\mathbf{E_{v_{i1}}}^T\,\mathbf{E_{v_{i1}}} + \mathbf{E_{\omega_{i1}}}^T\,\mathbf{I_{i1}}\,\mathbf{E}_{\boldsymbol{\omega}_{i1}}\right)\dot{\mathbf{q}} \\ &= \tfrac{1}{2}\,\dot{\mathbf{q}}^T\,\mathbf{M_{s_{i1}}}\,\dot{\mathbf{q}}, \end{aligned} \tag{35}$$

where $\mathbf{M_{s_{i1}}}$ is the inertia matrix of the cylinder.

The potential energy of the ith cylinder,

$$U_{s_{i1}} = m_{i1}\,g\,l_{ci_1}\,\sin\varphi_i. \tag{36}$$

Limbs-rod. The kinetic and potential energies of the rod are calculated following the same procedure described for the cylinder. In this case the center of mass of the ith rod is

$$\mathbf{CM}_{i2} = \mathbf{a_i} + \begin{bmatrix} (l_i - l_{ci_2}) & \cos\theta_i & \cos\varphi_i \\ (l_i - l_{ci_2}) & \sin\theta_i & \cos\varphi_i \\ & (l_i - l_{ci_2})\,\sin\varphi_i & \end{bmatrix}. \tag{37}$$

Thus, following the procedure described for the cylinder,

$$\begin{aligned} K_{s_{i2}} &= \tfrac{1}{2}\,\dot{\mathbf{q}}^T \left(m_{i2}\,\mathbf{E_{v_{i2}}}^T\,\mathbf{E_{v_{i2}}} + \mathbf{E}^T_{\boldsymbol{\omega}_{i2}}\,\mathbf{I_{i2}}\,\mathbf{E}_{\boldsymbol{\omega}_{i2}}\right)\dot{\mathbf{q}} \\ &= \tfrac{1}{2}\,\dot{\mathbf{q}}^T\,\mathbf{M_{s_{i2}}}\,\dot{\mathbf{q}}, \\ U_{s_{i2}} &= m_{i2}\,g\,(l_i - l_{ci_2})\,\sin\varphi_i. \end{aligned} \tag{38}$$

Lagrangian of the Gough platform. Combining the contributions of all the components of the robot,

$$\begin{aligned} L_S &= \frac{1}{2}\,\dot{\mathbf{q}}^T\,\mathbf{M_s}\,\dot{\mathbf{q}} \\ &\quad - \sum_{i=1}^{6}\left[m_{i2}\,(l_i - l_{ci_2}) + m_{i1}\,l_{ci_1}\right]\,g\,\sin\varphi_i, \\ L_{MP} &= \tfrac{1}{2}\,\dot{\mathbf{x}}^T\,\mathbf{M_x}\,\dot{\mathbf{x}} - (m_p + m_c)\,g\,z, \\ L &= L_{MP} + L_S, \end{aligned} \tag{39}$$

where $\mathbf{M_s} = \sum_{i=1}^{6}(\mathbf{M_{s_{i1}}} + \mathbf{M_{s_{i2}}})$.

3.8. Equations of motion

Using the Lagrange Multiplier formulation, the following equations of motion can be obtained from the Lagrangian Eq. (39):

$$\begin{aligned} \mathbf{D_x}\,\ddot{\mathbf{x}} + \mathbf{C_x}\,\dot{\mathbf{x}} + \mathbf{G_x} - \mathbf{Q_x} &= \left[\tfrac{\partial \Gamma(\mathbf{x},\mathbf{q})}{\partial \mathbf{x}}\right]^T\,\boldsymbol{\lambda}, \\ \mathbf{D_s}\,\ddot{\mathbf{q}} + \mathbf{C_s}\,\dot{\mathbf{q}} + \mathbf{G_s} &= \left[\tfrac{\partial \Gamma(\mathbf{x},\mathbf{q})}{\partial \mathbf{q}}\right]^T\,\boldsymbol{\lambda} + \boldsymbol{\tau_r}, \end{aligned} \tag{40}$$

where $\mathbf{D_x}$, $\mathbf{C_x}$, and $\mathbf{G_x}$ are the inertia, Coriolis, and gravity terms associated with the mobile platform, $\mathbf{D_s}$, $\mathbf{C_s}$, and $\mathbf{G_s}$ are the inertia, Coriolis, and gravity terms associated with the limbs, $\mathbf{Q_x}$ is the vector of external forces/torques applied to the mobile platform, $\boldsymbol{\lambda}$ is the vector of the Lagrange multipliers, and $\tau_{r_j}]_{j=1,\ldots 6} = \boldsymbol{\tau_r}$ are the virtual torques that would be applied at all the joints of the mechanism if all were actuated.

3.9. Dynamic model

Once the equations of motion of both subsystems have been obtained, the dynamic model can be expressed in terms of the control coordinates $\mathbf{q_c}$, i.e., in the joint space, or in terms of the output coordinates $\mathbf{x}$, i.e., in the task space.

Solving Eq. (40),

$$\begin{aligned} \boldsymbol{\tau_r} &= \mathbf{D_s}\ddot{\mathbf{q}} + \mathbf{C_s}\dot{\mathbf{q}} + \mathbf{G_s} \\ &\quad \underbrace{-\left(\frac{\partial \boldsymbol{\Gamma}}{\partial \mathbf{q}}\right)^T}_{6\times 6}\underbrace{\left[\left(\frac{\partial \boldsymbol{\Gamma}}{\partial \mathbf{x}}\right)^T\right]^{\dagger}}_{6\times 3}(\mathbf{D_x}\,\ddot{\mathbf{x}} + \mathbf{C_x}\,\dot{\mathbf{x}} + \mathbf{G_x} - \mathbf{Q_x}). \end{aligned} \tag{41}$$

As the partial derivatives of the constraint equation $\boldsymbol{\Gamma}(\mathbf{x},\mathbf{q}) = \mathbf{0}_{18\times 1}$ (Eq. (3)) are equal to the transpose of the constraint Jacobian of the robot $\mathbf{J_C} = \partial\mathbf{x}/\partial\mathbf{q}$,

$$\begin{aligned} \boldsymbol{\tau_r} &= \mathbf{D_s}\,\ddot{\mathbf{q}} + \mathbf{J}_C^T\,\mathbf{D_x}\,\ddot{\mathbf{x}} + \mathbf{C_s}\,\dot{\mathbf{q}} + \mathbf{J}_C^T\,\mathbf{C_x}\,\dot{\mathbf{x}} + \mathbf{G_s} \\ &\quad + \mathbf{J}_C^T\,\mathbf{G_x} - \mathbf{J}_C^T\,\mathbf{Q_x}, \end{aligned} \tag{42}$$

https://doi.org/10.1017/S0263574712000185 Published online by Cambridge University Press

where $\boldsymbol{\tau_r}$ is the set of virtual forces and torques associated with all the joint variables $\mathbf{q}$. In order to project the dynamic model into the actuator space $\boldsymbol{\tau}_{q_a}$, the Jacobian matrix $\mathbf{T}$, Eq. (23), is used:[34]

$$\boldsymbol{\tau}_{q_a} = \mathbf{T}^T \boldsymbol{\tau}_r. \tag{43}$$

The dynamic model as stated in Eq. (43) is expressed in terms of the output coordinates $\mathbf{x}$ and all the joint coordinates $\mathbf{q}$. Using the kinematic relations defined in Sections (3.5) and (3.6), this model can be re-expressed in terms of the control coordinates $\mathbf{q_c}$,

$$\boldsymbol{\tau}_{q_a} = \mathbf{D}\ddot{\mathbf{q}}_\mathbf{c} + \mathbf{C}\dot{\mathbf{q}}_\mathbf{c} + \mathbf{G} + \mathbf{F_{ext}}, \tag{44}$$

where

$$\mathbf{D} = \mathbf{T}^T \mathbf{D_q} \mathbf{T_q} + \left[\mathbf{J_{q_a}}^{-1}\right]^T \mathbf{D_x} \mathbf{J}_p,$$
$$\mathbf{C} = \mathbf{T}^T \left(\mathbf{D_q} \dot{\mathbf{T}}_\mathbf{q} + \mathbf{C_q} \mathbf{T_q}\right) + \left[\mathbf{J_{q_a}}^{-1}\right]^T \left(\mathbf{D_x} \dot{\mathbf{J}}_p + \mathbf{C_x} \mathbf{J_p}\right),$$
$$\mathbf{G} = \mathbf{T}^T \mathbf{G_q} + \left[\mathbf{J_{q_a}}^{-1}\right]^T \mathbf{G_x},$$
$$\mathbf{F_{ext}} = -\left[\mathbf{J_{q_a}}^{-1}\right]^T \mathbf{Q_x},$$

where $\mathbf{T}^T \mathbf{J_C}^T = [\mathbf{J_{q_a}}^{-1}]^T$.

Similarly, the dynamic model can be defined in the task space.

Note that in order to calculate the inverse dynamic model (IDM) in both joint and task spaces, a generic set of control coordinates $\mathbf{q_c}$ has been used. Moreover, the Jacobians used to project the inverse dynamic model into the actuator space are defined in terms of the selection vector $\mathbf{I_c}$, which also defines the set of control coordinates. This makes it possible to derive the dynamic model once, and define it in terms of different sets of $\mathbf{q_c}$ by defining different selection vectors $\mathbf{I_c}$ without the need to rederive the model. Thus, this dynamic model can be used to analyze the effect of different sensor configurations with minimum effort.

It must be noted, however, that as in non-redundant dynamic models, this dynamic model is only defined when the Jacobian matrices used to calculate it are not singular, that is, when no direct kinematic singularities arise. This is a generalized problem when modelling parallel robots, regardless of the coordinates used in $\mathbf{q_c}$.[17] Thus, a singularity-free safe region should be defined.

4. Validation of the Redundant Dynamic Model of the Gough Platform

As stated in the Introduction, the Gough platform, being one of the most popular parallel robots, has been the subject of extensive research. In the dynamics field, the papers by Wang and Gosselin,[42] Tsai,[41] and Guo and Li[19] provide a complete example suitable for model validation and we applied it here to the redundant dynamic modelling procedure.

The parameters of the dynamic model used for validation in the aforementioned papers are summarized in Table II.

In order to validate the dynamic model, the two reference trajectories proposed in the previously referenced papers will be used in order to compare the results obtained. The first one

Table II. Dynamic and kinematic parameters ($i = 1 \ldots 6$).

Parameter	value
$\mathbf{a_1}$	$[-2.12 \quad 1.374 \quad 0]^T$ (m)
$\mathbf{a_2}$	$[-2.38 \quad 1.224 \quad 0]^T$ (m)
$\mathbf{a_3}$	$[-2.38 \quad -1.224 \quad 0]^T$ (m)
$\mathbf{a_4}$	$[-2.12 \quad -1.374 \quad 0]^T$ (m)
$\mathbf{a_5}$	$[0 \quad -0.15 \quad 0]^T$ (m)
$\mathbf{a_6}$	$[0 \quad 0.15 \quad 0]^T$ (m)
$\mathbf{d_1}$	$[0.17 \quad 0.595 \quad -0.4]^T$ (m)
$\mathbf{d_2}$	$[-0.6 \quad 0.15 \quad -0.4]^T$ (m)
$\mathbf{d_3}$	$[-0.6 \quad -0.15 \quad -0.4]^T$ (m)
$\mathbf{d_4}$	$[0.17 \quad -0.595 \quad -0.4]^T$ (m)
$\mathbf{d_5}$	$[0.43 \quad -0.445 \quad -0.4]^T$ (m)
$\mathbf{d_6}$	$[0.43 \quad 0.445 \quad -0.4]^T$ (m)
l_{i1}	0.5 (m)
lc_{l_i1}	0.25 (m)
l_{i2}	0.5 (m)
lc_{l_i2}	0.25 (m)
m_p	1.5 (kg)
m_c	0 (kg)
m_{i1}	0.1 (kg)
m_{i2}	0.1 (kg)
$\mathbf{I_p}$	$0.08\,\mathbf{I_3}$ (kg m^2)
$\mathbf{I_{i1}}$	$0.00625\,\mathbf{I_3}$ (kg m^2)
$\mathbf{I_{i2}}$	$0.00625\,\mathbf{I_3}$ (kg m^2)
$\mathbf{I_c}$	$\mathbf{0_3}$ (kg m^2)

is a constant orientation trajectory, where $\alpha = \beta = \gamma = 0$, and

$$\mathbf{p_x} = \begin{bmatrix} -1.5 + 0.2 \sin \omega t \\ 0.2 \sin \omega t \\ 1 + 0.2 \sin \omega t \end{bmatrix},$$

where $\omega = 3$ rad/s and $\omega t = [0, 2\pi]$.

The second trajectory is a constant position trajectory where $\mathbf{p_x} = [-1.5 \; 0 \; 1]^T$ and the platform rotates with respect to the fixed z-axis: $\alpha = \beta = 0$ and $\gamma = 0.35 \sin \omega t$ with $\omega = 3$ rad/s and $\omega t = [0, 2\pi]$.

The forces required to execute the proposed reference trajectories are shown in Figs. 7 and 8. These values have been calculated for the case in which $\mathbf{q_c} = \mathbf{q}$, i.e., all joint variables are considered to be measurable. Comparing the way the force varies with time for two trajectories with the work of Wang and Gosselin,[42] Tsai,[41] and Guo and Li,[19] no significant differences can be appreciated. That is, for the same reference trajectories and model parameters, the redundant dynamic model yields same results as those obtained by the cited authors.

Moreover, it can be demonstrated that, as could be expected, for any set of control coordinates $\mathbf{q_c}$ selected to execute the reference trajectories, the required forces are the same.

5. Validation of the Extended CTC approach applied to the Gough Platform

In this section, the Extended CTC control approach is applied to the Gough platform in order to assess whether

https://doi.org/10.1017/S0263574712000185 Published online by Cambridge University Press

Table III. Extended CTC configurations.

Config.	$\mathbf{q_c}$
1	$\mathbf{q_c} = \mathbf{q_a} \in \mathbb{R}^6$
2	$\mathbf{q_c} = [\,\mathbf{q_a}^T\ \theta_1\ \theta_3\ \varphi_1\ \varphi_3\,]^T \in \mathbb{R}^{10}$
3	$\mathbf{q_c} = [\,\mathbf{q_a}^T\ \varphi^T\,]^T \in \mathbb{R}^{12}$
4	$\mathbf{q_c} = \mathbf{q} \in \mathbb{R}^{18}$

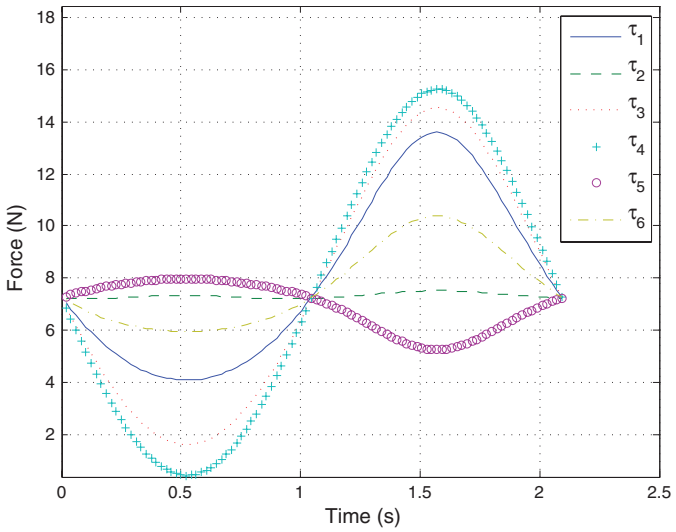


Fig. 7. (Colour online) Forces for the constant orientation trajectory.

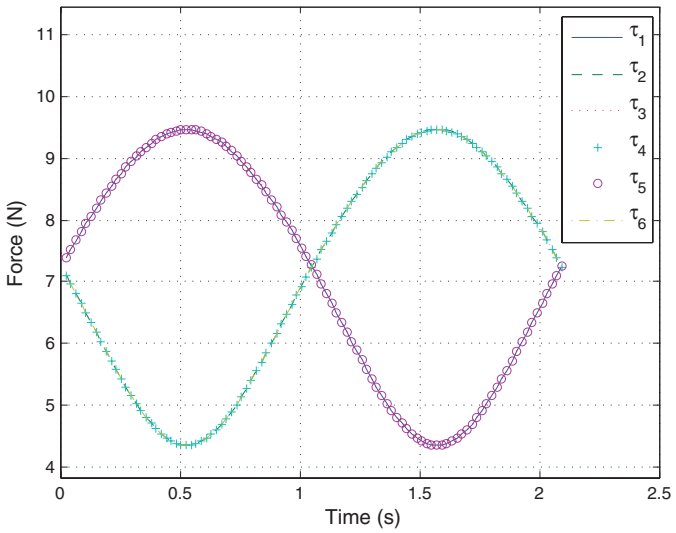


Fig. 8. (Colour online) Forces for the constant position trajectory.

it has advantages over the classical, non-redundant CTC approach. For that purpose, the Extended CTC scheme has been implemented in Matlab/Simulink in both joint and task spaces using the previously validated redundant dynamic model.

The set of experiments is carried out considering the four different sensor configurations summarized in Table III.

Three reference trajectories are defined in the task space for the set of simulations. The trajectories with constant position and orientation are defined in Section 4, and a complex, high-speed helicoidal trajectory is defined in the non-singular workspace of the Gough platform (Fig. 9). This

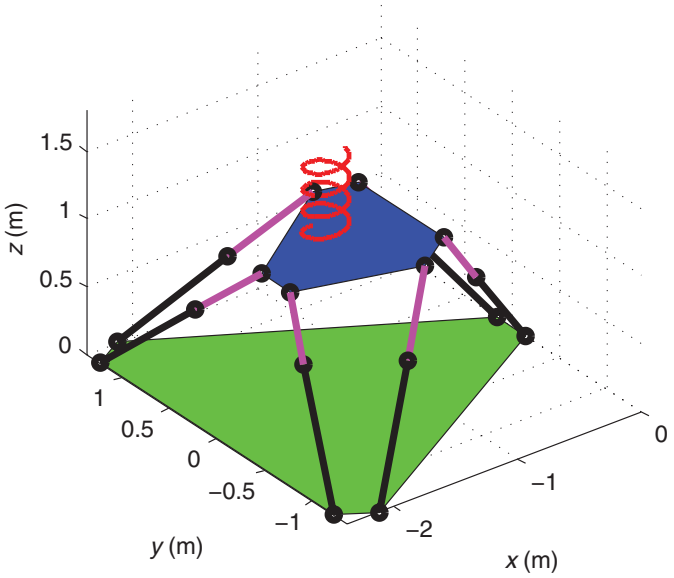


Fig. 9. (Colour online) Helicoidal reference trajectory.

final trajectory allows the controller to be tested in a wide workspace area (Eq. 45),

$$\mathbf{x_{ref}} = \begin{bmatrix} 0.4\,\cos(10\,t) \\ 0.4\,\sin(10\,t) \\ 1.2 + 0.1592\,t \\ 10\,\pi/180\,\sin(12\,t) \\ 10\,\pi/180\,\cos(12\,t) \\ 10\,\pi/180\,\sin(12\,t) \end{bmatrix} \tag{45}$$

The comparative analysis of control schemes consists in studying the control performance of the TCP tracking error obtained by each scheme. In order to assess the control performance, the Integral of the Absolute Error (IAE) performance index of the end-effector positioning and orientation error, defined as $\int_0^\infty |e(t)|dt$, will be analyzed. Specifically, for the proposed reference trajectories, the real end-effector coordinates $\mathbf{x}$ are measured and compared with the desired ones in order to calculate the tracking accuracy.

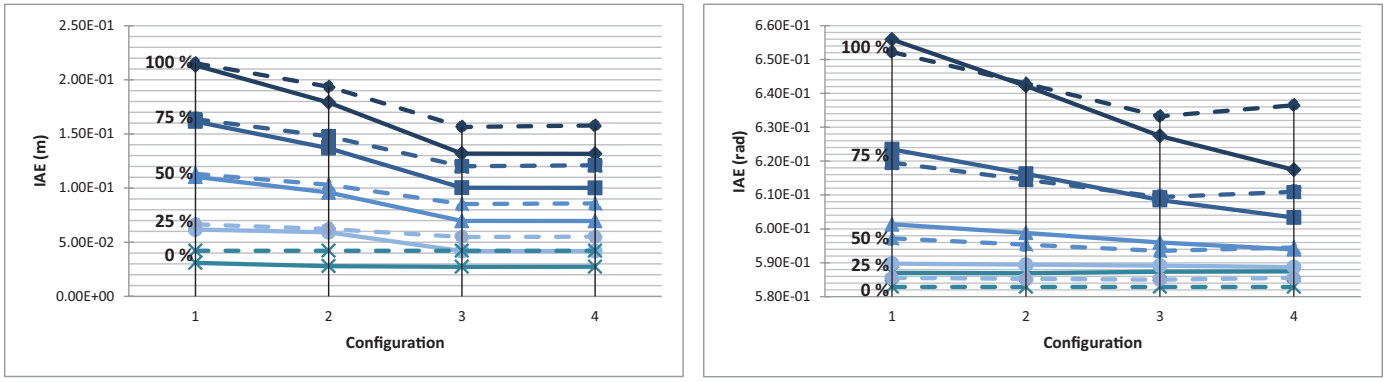
The model parameter set used for simulations are detailed in Table II, where a load of mass $m_c = 1$ kg and inertia $\mathbf{I_c} = 0.06\,\mathbf{I_3}$ kg m^2 is attached to the platform. In addition, a friction term $\mathbf{F_r}$ is introduced into the direct dynamic model to simulate the dynamics of the robot,

$$\boldsymbol{\tau} = \mathbf{D}\ddot{\mathbf{q}}_\mathbf{c} + \mathbf{C}\dot{\mathbf{q}}_\mathbf{c} + \mathbf{G} + \mathbf{F_{ext}} + \mathbf{F_r}, \tag{46}$$

where the friction term $\mathbf{F_r} = \mathbf{T}^T\mathbf{F_v}\,\dot{\mathbf{q}} + \mathbf{T}^T\,\mathbf{F_c}\,sign(\dot{q})$ is composed of a viscous friction term $\mathbf{F_v}$ and a Coulomb friction term $\mathbf{F_c}$, $\mathbf{F_v}$ and $\mathbf{F_c}$ being diagonal matrices. The $\mathbf{F_v}$ terms associated with active joints $\mathbf{q_a}$ are assigned a value of 0.83 kg m/s, and those associated with the non-actuated joints are assigned a value of 0.09 kg m/s. Further, the terms of $\mathbf{F_c}$ associated with the active joints $\mathbf{q_a}$ are 0.42 N , while those associated with the non-actuated joints are 0.05 N.

The proportional K_p and velocity K_v gains of the classical CTC controller have been tuned to obtain a maximum

https://doi.org/10.1017/S0263574712000185 Published online by Cambridge University Press



(a) (b)

Fig. 10. (Colour online) Orientation Constant Trajectory. Average IAE (JS solid, TS dashed). (a) Orientation constant Traj. IAE in the position; (b) orientation constant traj. IAE in the orientation.

Table IV. Maximum errors.

Distance	0.001 m
Mass	0.01 kg
Inertia	10% of nominal value

overshoot of 5% and a peak time of 0.05 s. The same gains are used for all controllers, and the cycle time is set to 5 ms.

In order to show the effect of parameter uncertainty in the model identification, the real robot parameters have been randomly modified from their nominal values by a maximum value. For this purpose, five different variation values have been used, linearly distributed from 0% error to maximum errors (100%) specified in Table IV.

In addition, in order to obtain statistical data, each simulation iteration has been repeated 350 times for each case using different variation templates. For this purpose, as a first step the parameter modification templates are created, that is, each model parameter (length, inertia, and mass) is randomly assigned a 0, –1, or 1 value, meaning no value change, increment in its nominal value, or decrement in its nominal value by the variation value selected, respectively. These templates are generated randomly, one for each simulation iteration. Thus, for each parameter variation value and simulation iteration, the modified parameters are calculated using the predefined templates. For a given variation value (%), the average behavior of the controller in each set of iterations is considered.

In Figs. 10–12 the results of the comparative study for each reference trajectory are shown. As would be expected, the performance index increases with parameter variation, that is, errors increase when parameter uncertainties are higher for all controllers; on the other hand, both the relative increase and the absolute values of the IAE are different for each configuration. Thus, from the analysis of these figures, three important conclusions can be drawn.

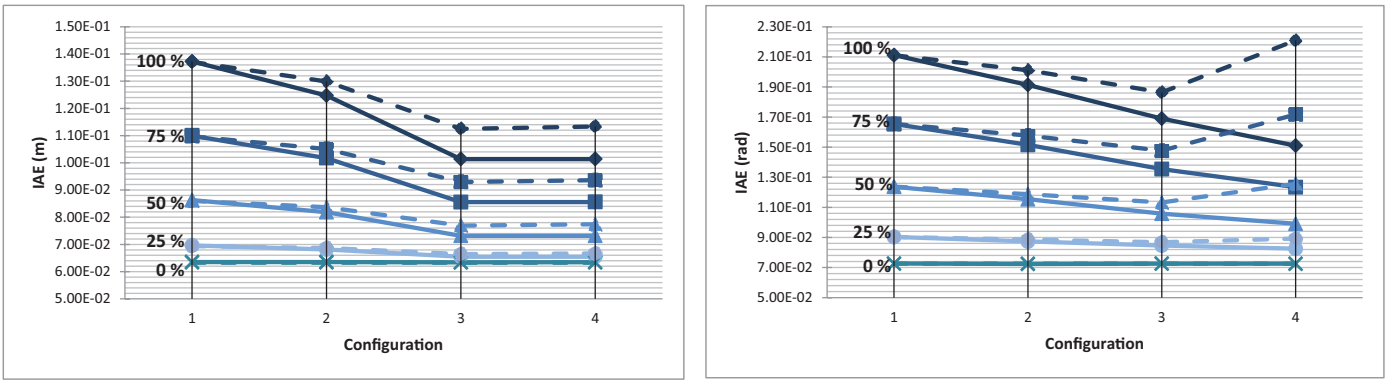
First, as expected, the use of different sensor configurations varies the performance of the Extended CTC approach. As can be seen in the aforementioned figures, in the general case, the performance is better with the redundant configurations (2, 3, and 4) than the classical CTC controller (configuration 1) when parameter errors arise. Moreover, if only the positioning error is considered for three reference trajectories, it can be clearly seen that configuration 4, which requires that all joints are sensorized, provides the best performance in both joint and task spaces. However, this approach increases the hardware cost, as 12 extra sensors are needed. Thus, if hardware costs are also considered, configuration 3, which only requires six extra sensors, achieves a good cost-performance ratio.

Second, the implementation space of the controller is a key issue in its performance. As can be seen in the results, the task and joint space implementations of a given Extended CTC configuration do not provide same results. Moreover, the results clearly show that the joint space implementation has better performance on average than the task space implementation when error parameters arise. In addition, the differences between two implementations increase with model parameter errors. This effect is due to the fact that when implementing the model in the joint space, the redundant information, the control coordinates, are directly and explicitly used in the controller, making it more robust than the task space implementation.

Third, the use of extra sensor data does not always guarantee better results. This fact can be clearly seen in the trend in the IAE in the orientations of Figs. 10 and 11. In these cases, all joints being sensorized do not provide better results than the classical CTC approach. Moreover, configurations 2 and 3, which are redundant and require fewer extra sensors, provide better results when parameter uncertainties are high. Thus, it is clear that it is necessary to identify an appropriate sensor distribution to achieve the best performance and exploit the potential of the Extended CTC approach.

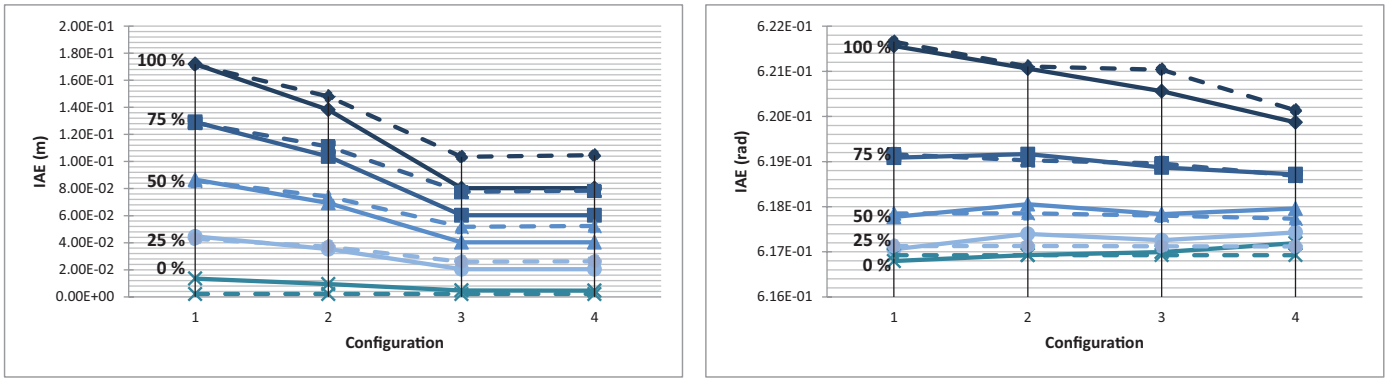
As a more detailed example, in Fig. 13 the error over time associated with two TCP locations is shown for a case in which a helicoidal trajectory is followed and maximum errors are introduced in nominal parameters. For this, configuration 1, which is equivalent to the classical CTC, and configuration 4, in which all joints have sensors, have been selected to illustrate differences between the approaches. A joint-space implementation is used. Results show that the trajectory tracking error is smaller in the redundant case (configuration 4) than the non-redundant one (configuration 1). Consistent with the trends shown in Figs. 10–12, this example illustrates the effectiveness of the proposed approach.

https://doi.org/10.1017/S0263574712000185 Published online by Cambridge University Press



(a) (b)

Fig. 11. (Colour online) Position constant trajectory. Average IAE (JS solid, TS dashed). (a) Position constant traj. IAE in the position; (b) position constant traj. IAE in the orientation.



(a) (b)

Fig. 12. (Colour online) Helicoidal constant trajectory. Average IAE index (JS solid, TS dashed). (a) Helicoidal traj. positioning error IAE; (b) helicoidal constant traj. orientation error IAE.

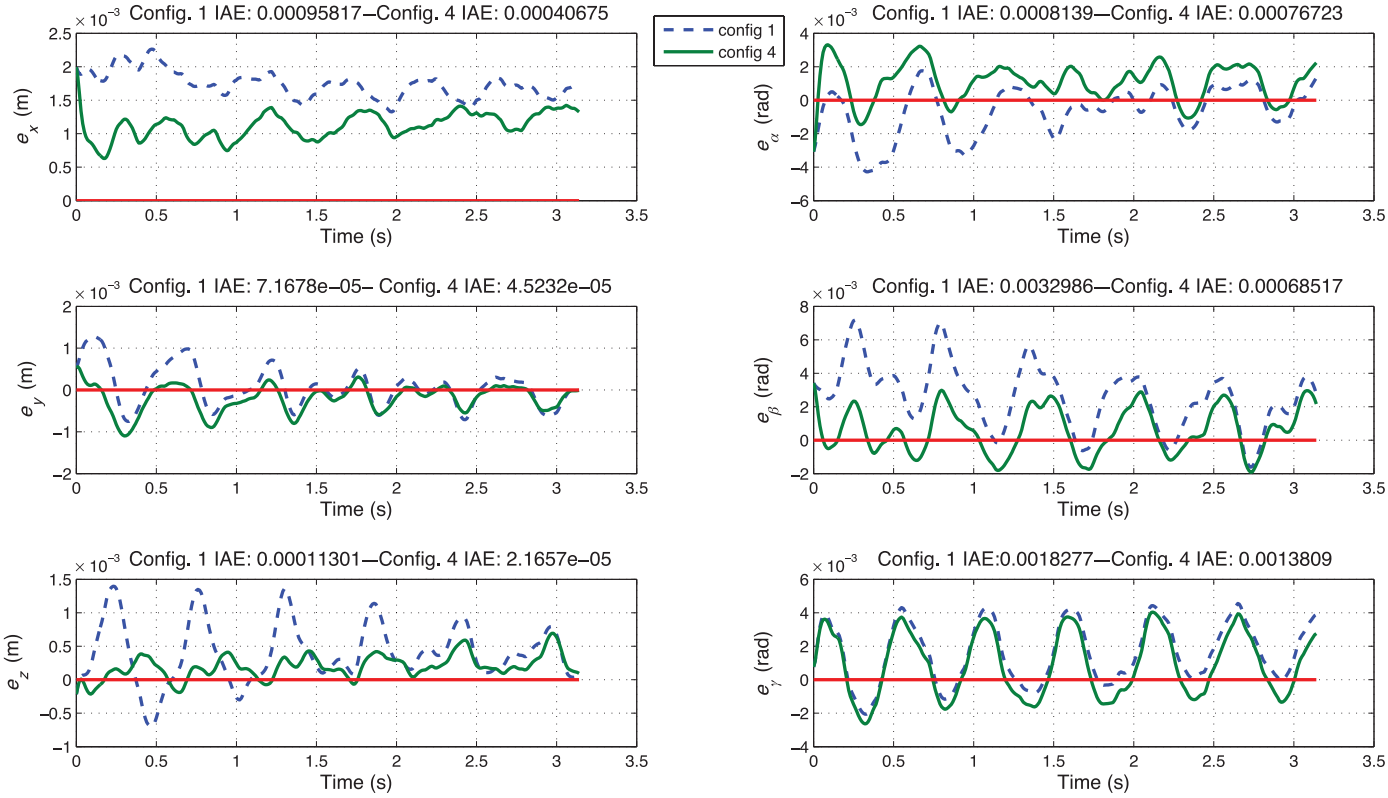


Fig. 13. (Colour online) Time evolution of the TCP position and orientation error.

https://doi.org/10.1017/S0263574712000185 Published online by Cambridge University Press

Thus, in summary, it has been demonstrated that the use of redundant Extended CTC configurations can provide better performance than the classical CTC approaches even in the presence of model parameter errors and nonlinear phenomena such as friction. However, it is clear that in order to achieve the best results, the sensor configuration has to be selected with care.

6. Conclusions

Current robotic applications require high-speed operation with accurate trajectory tracking and positioning. Parallel robots can fulfill these requirements, but to do so need model-based control schemes that, in turn, tend to rely on an accurate dynamic model. All this is, in general, difficult to achieve, as parameter identification errors arise and simplifications are usually made, which decrease the performance of model-based controllers. In order to increase the performance of the control loop in high-speed applications, the use of sensors in some passive joints is proposed. Although this approach increases hardware costs, the extra data allow trajectory tracking errors to be reduced and may decrease the computational cost of the model.

This paper makes two main contributions. First, a redundant dynamic modelling approach for the Gough platform is presented. The redundant dynamic model derived allows the data from some extra sensorized joints to be used in kinematic and dynamic equations. This way, the model obtained is more robust against model parameter uncertainty and enables better estimation of unmeasurable variables, such as TCP position.

Secondly, a redundant control approach based on the aforementioned dynamic model is proposed. This approach, termed as the Extended CTC, is a generalization of the classical CTC approach and uses the redundant dynamic model in order to define the control law in terms of both active joints and some extra sensorized joints. If an appropriate sensor configuration is selected, this scheme makes it possible to significantly reduce the effect of model parameter uncertainty, providing better control performance than the classical CTC approach.

Both the redundant dynamic modelling procedure and the Extended CTC approaches are validated using simulation experiments. For dynamic modelling, the approach is validated by comparing the formulation results with those obtained by other authors. On the other hand, the Extended CTC approach is tested by means of a set of experiments in which randomly generated errors are introduced in the dynamic model. Simulation results demonstrate that performance indices considering the trajectory tracking error of the TCP when parameter uncertainties arise can be improved, and this validates the proposed approach.

Acknowledgments

This work was funded by the Spanish Ministry of Science and Innovation and ERDF under projects DPI-2009-07669 and DPI 2008-00159, and the University of the Basque Country (UPV/EHU) under grants GIU10/20 and IT445-10.

References

1. H. Abdellatif and B. Heimann, "Computational efficient inverse dynamics of 6-dof fully parallel manipulators by using the lagrangian formalism," *Mech. Mach. Theory* **44**, 192–207 (2009).
2. J. Angeles, *Fundamentals of Robotic Mechanical Systems: Theory, Methods, and Algorithms* (Springer, New York, 2007).
3. R. Aracil, R. Saltaren and O. Reinoso, "A climbing parallel robot: A robot to climb along tubular and metallic structures," *Robot. Autom. Mag.* **13**(1), 16–22 (2006).
4. L. Baron and J. Angeles, "The kinematic decoupling of parallel manipulators using joint-sensor data," *IEEE Trans. Robot. Autom.* **16**(6), 644–651 (2000).
5. V. Bauma, M. Valášek and Z. Sika, "Increase of PKM Positioning Accuracy by Redundant Measurement," **In**: *Proceedings of the 5th Chemnitzer Parallel Kinematik Seminar*, Chemnitz, Germany (2006) pp. 547–564.
6. S. Bhattacharya, H. Hatwal and A. Ghosh, "An on-line parameter estimation scheme for generalized stewart platform-type parallel manipulators," *Mech. Mach. Theory* **32**(1), 79–89 (1997).
7. S. Bhattacharya, N. Nenchev and M. Uchiyama, "A recursive formula for the inverse of the inertia matrix of a parallel manipulator," *Mech. Mach. Theory* **33**(7), 957–964 (1998).
8. I. Cabanes, A. Zubizarreta, M. Marcos and C. Pinto, "Real Time Distributed Control of Parallel Robots Using Redundant Sensors," **In**: *Proceedings of the 40th International Symposium on Robotics*, Barcelona, Spain (2009) pp. 139–144.
9. B. Dasgupta and T. Mruthyunjaya, "A Newton--Euler formulation for the inverse dynamics of the stewart platform," *Mech. Mach. Theory* **33**(8), 1135–1152 (1998).
10. B. Dasgupta and T. Mruthyunjaya, "The stewart platform manipulator: A review," *Mech. Mach. Theory* **35**(1), 15–40 (2000).
11. W. Q. D. Do and D. C. H. Yang, "Inverse dynamic analysis and simulation of a platform type of robot," *J. Robot. Syst.* **5**(3), 209–227 (1988).
12. T. Dwarakanath, B. Dasgupta and T. Mruthyunjaya, "Design and development of a stewart platform-based force-torque sensor," *Mechatronics* **11**(7), 793–809 (2001).
13. S. Fu and Y. Ya, "Non-linear robust control with partial inverse dynamic compensation for a stewart platform manipulator," *Int. J. Modelling Identif. Control* **1**(1), 44–51 (2006).
14. J. Gallardo, J. M. Rico, A. Frisoli, D. Checcacci and M. Bergamasco, "Dynamics of parallel manipulators by means of screw theory," *Mech. Mach Theory* **38**, 1113–1131 (2003).
15. T. Geike and J. McPhee, "Inverse dynamic analysis of parallel manipulators with full mobility," *Mech. Mach. Theory* **38**, 549–562 (2003).
16. A. Ghobakhloo, M. Eghtesad and M. Azadi, "Position Control of a Stewart–Gough Platform Using Inverse Dynamics Method with Full Dynamics," **In**: *Proceedings of the 9th IEEE International Workshop on Advanced Motion Control*, Istanbul, Turkey (2006) pp. 50–55 .
17. F. Ghorbel, O. Chételat, R. Gunawardana and R. Longchamp, "Modeling and set point control of closed-chain mechanisms: Theory and experiment," *IEEE Trans. Control Syst. Tech.* **8**(5), 801–815 (2000).
18. V. Gough and S. Whitehall, "Universal Tyre Test Machine," **In**: *Proceedings of the FISITA Ninth International Technical Congress*, London (May, 1962) pp. 117–137 .
19. H. Guo and H. Li, "Dynamic analysis and simulation of a six degree of freedom stewart platform manipulator," *Proc. IMechE C: J. Mech. Eng. Sci.* **220**, 61–72 (2006).
20. H. B. Guo, Y. Liu, G. Liu and H. Li, "Cascade control of a hydraulically driven 6-DOF parallel robot manipulator based on a sliding mode," *Control Eng. Pract.* **16**(9), 1055–1068 (2008).
21. B. R. Hopkins and R. L. Williams II, "Kinematics, design and control of the 6-psu platform," *Ind. Robot Int. J.* **29**(5), 443–451 (2002).

https://doi.org/10.1017/S0263574712000185 Published online by Cambridge University Press

22. C.-I. Huang, C.-F. Chang, M.-Y. Yu and L.-C. Fu, "Sliding-mode tracking control of the stewart platform," *5th Asian Control Conf.* **1**, 562–569 (2004).
23. S. Iqbal, A. I. Bhatti and Q. Ahmed, "Dynamic Analysis and Robust Control Design for Stewart Platform with Moving Payloads," **In**: *Proceedings of the 17th World Congress of the International Federation of Automatic Control (IFAC 2008)*, COEX, South Korea (2008) pp. 5324–5329.
24. W. Khalil and S. Guegan, "Inverse and direct dynamic modeling of gough-stewart robots," *IEEE Trans. Robot* **20**(4), 754–762 (2004).
25. D. H. Kim, J-Y. Kang and K.-I. Lee, "Robust tracking control design for a 6 dof parallel manipulator," *J. Robot. Syst.* **17**(10), 527–547 (2000).
26. N.-I. Kim and C.-W. Lee, "High-Speed Tracking Control of Stewart Platform Manipulator via Enhanced Sliding Mode Control," **In**: *Proceedings of the IEEE International Conference in Robotics and Automation*, Leuven, Belgium (May 1998) pp. 2716–2721.
27. G. Lebret, K. Liu and F. L. Lewis, "Dynamic analysis and control of a stewart platform manipulators," *J. Robot. Syst.* **10**(5), 629–655 (1993).
28. S.-H. Lee, J.-B. Song, W.-C. Choi and D. Hong, "Position control of a stewart platform using inverse dynamics control with approximate dynamics," *Mechatronics* **13**, 605–619 (2003).
29. D. Li and S. Salcudean, "Modeling, simulation and control of a hydraulic stewart platform," *IEEE Int. Conf. Robot. Autom.* **4**, 3360–3366 (1997).
30. F. Marquet, O. Company, S. Krut and F. Pierrot, "Enhancing Parallel Robots Accuracy with Redundant Sensors," **In**: *Proceedings of the 2002 IEEE International Conference on Robotics and Automation*, Minnesota, USA (2002) pp. 4114–4119.
31. J. P. Merlet, "Closed form resolution of the direct kinematics of parallel manipulators using extra sensors data," **In:** *Proceedings of the IEEE International Conference in Robotics and Automation*, Atlanta, GA (1993) pp. 200–304.
32. J. P. Merlet," *Parallel Robots,* 2nd. ed (Kluwer, London, UK, 2006).
33. R. Nakadate, H. Uda, H. Hirano, J. Solis, A. Takanishi, E. Minagawa, M. Sugawara and K. Niki, "Development of a Robotic Carotid Blood Measurement Wta-1rii: Mechanical Improvement of Gravity Compensation Mechanism and Optimal link Position of the Parallel Manipulator Based on ga," **In:** *Proceedings of the IEEE/ASME International Conference on Advanced Intelligent Mechatronics*, Singapore (Jul. 2009) pp. 717–722.
34. Y. Nakamura and M. Godoussi, "Dynamics computation of closed-link robot mechanisms with nonredundant and redundant actuators," *IEEE Trans. Robot. Autom.* **5**(3), 294–302, (1989).
35. A. Omran, G. El-Bayiumi, M. Bayoumi and A. Kassem, "Genetic algorithm-based optimal control for a 6-DOF non-redundant Stewart manipulator," *Int. J. Mech. Ind. Aerosp. Eng.* **2**(2), 73–79 (2008).
36. V. Parenti-Castelli and R. D. Gregorio, "A new algorithm based on two extra-sensors for real-time computation of the actual configuration of the generalized Stewart-Gough manipulator," *J. Mech. Des.* **122**(1), 294–298 (2000).
37. S. Riebe and H. Ulbrich, "Modelling and online computation of the dynamics of a parallel kinematic with six degrees-of-freedom," *Arch. Appl. Mech.* **72**, 813–829 (2003).
38. D. Stewart, "A platform with six degrees of freedom," *Proc. IMechE* **180**, 371–385 (1965-1966).
39. Y. Su and B. Duan, "The application of the Stewart platform in large spherical radio telescopes," *J. Robot. Syst.* **17**(7), 375–383 (2000).
40. Y. X. Su, B. Y. Duan, C. H. Zheng, Y. F. Zhang, G. D. Chen and J. W. Mi, "Disturbance-rejection high-precision motion control of a stewart platform," *IEEE Trans. Control Syst. Tech.* **12**(3), 364–374 (2004).
41. L.-W. Tsai, "Solving the inverse dynamics of a Stewart-Gough manipulator by the principle of virtual work," *ASME J. Mech. Des.* **122**, 3–9 (2000).
42. J. Wang and C. Gosselin, "A new approach for the dynamic analysis of parallel manipulator," *Multibody Syst. Dyn.* **2**, 317–334 (1998).
43. C. Yang, Q. Huang, H. Jiang, O. O. Peter and J. Han, "Pd control with gravity compensation for hydraulic 6-dof parallel manipulator," *Mech. Mach. Theory* **45**(4), 666–677 (2010).
44. A. Zubizarreta, I. Cabanes, M. Marcos and C. Pinto, "Control of Parallel Robots Using Passive Sensor Data," **In**: *Proceedings of the IEEE/RSJ International Conference on Intelligent Robots and Systems, (IROS 2008)*, Nice, France (Sep. 22–26, 2008) pp. 2398–2403 .
45. C. Álvarez, R. Saltarén, R. Aracil and C. García, "Concepción, desarrollo y avances en el control de navegación de robots submarinos paralelos: El robot remo-i," *Revista Iberoamericana de Automática e Informática* **6**(3), 92–100 (2009) (in Spanish).

https://doi.org/10.1017/S0263574712000185 Published online by Cambridge University Press